Cryogenics 80 (2016) 52–62

Contents lists available at ScienceDirect

Cryogenics

journal homepage: www.elsevier.com/locate/cryogenics

Research paper

Numerical investigation of transient behaviour of the recuperative heat exchanger in a MR J–T cryocooler using different heat transfer correlations

R.M. Damle [a], P.M. Ardhapurkar [b], M.D. Atrey [a,*]

[a] Refrigeration and Cryogenics Laboratory, Department of Mechanical Engineering, Indian Institute of Technology Bombay, Powai, Mumbai 400076, Maharashtra, India
[b] S.S.G.M. College of Engineering, Shegaon 444203, India

ARTICLE INFO

Article history:
Received 4 July 2016
Received in revised form 8 September 2016
Accepted 8 September 2016
Available online 13 September 2016

Keywords:
J–T cryocooler
Transient
Mixed-refrigerant
Heat-exchanger

ABSTRACT

In J–T cryocoolers operating with mixed refrigerants (nitrogen-hydrocarbons), the recuperative heat exchange takes place under two-phase conditions. Simultaneous boiling of the low pressure stream and condensation of the high pressure stream results in higher heat transfer coefficients. The mixture composition, operating conditions and the heat exchanger design are crucial for obtaining the required cryogenic temperature. In this work, a one-dimensional transient algorithm is developed for the simulation of the two-phase heat transfer in the recuperative heat exchanger of a mixed refrigerant J–T cryocooler. Modified correlation is used for flow boiling of the high pressure fluid while different condensation correlations are employed with and without the correction for the low pressure fluid. Simulations are carried out for different mixture compositions and numerical predictions are compared with the experimental data. The overall heat transfer is predicted reasonably well and the qualitative trends of the temperature profiles are also captured by the developed numerical model.

1. Introduction

In a Joule–Thomson (J–T) cryocooler, precooling of the high pressure fluid stream before expansion is indispensable for limiting the maximum working pressure. This precooling is usually achieved, with the return fluid stream at lower temperature and pressure, in a counter flow recuperative heat exchanger. Typically, depending on the application, the operational pressures for J–T cryocoolers can be of the order of 100–200 bar with single component working fluids such as nitrogen and argon. However, with gas mixtures of nitrogen and hydrocarbons, the operational pressures can be brought down to 15–20 bar for obtaining cryogenic temperatures. Also, as compared to nitrogen as the working fluid, the J–T cryocooler efficiency increases with gas mixtures of nitrogen and hydrocarbons [1–4]. In case of mixtures, the heat transfer in the recuperative heat exchanger takes place in the liquid-vapour dome due to the boiling of low pressure stream and condensation of the high pressure stream. The two-phase flow enhances the heat transfer coefficients as compared to single phase heat exchange. Therefore, the heat transfer area requirement reduces which results in a smaller heat exchanger. Moreover, by adjusting the mixture composition it is possible to obtain cryogenic temperatures in the range of 80–120 K suitable for cooling infrared sensors and electronic devices, cryo-preservation, gas chillers, etc.

Numerous studies have been reported on mixed refrigerant Joule–Thomson (MR J–T) cryocoolers. A majority of these studies are dedicated to the optimization of mixture composition and thermodynamical aspects of the refrigeration system with mixed refrigerants [1–7]. Maytal [8] carried out experiments with two different mixtures and four different constructions of the J–T cryocooler to see their effect on the cool down time and cold end temperature. Tzabar [9] presented experiments with binary mixtures of nitrogen and hydrocarbons and included methods to predict the cooling temperature and the cooling power of the J–T cryocooler. Very few studies in the literature are dedicated to the analysis of the recuperative heat exchanger. Gong et al. [10] reported temperature profiles and pressure drop for a tubes-in-tube heat exchanger. Nellis et al. [11] carried out experiments under various operating conditions to obtain flow boiling heat transfer coefficients for mixed refrigerants. Alexeev et al. [12] conducted numerical studies on a tubes-in-tube heat exchanger with different gas mixtures. Ardhapurkar et al. [13] also carried out numerical analysis using global energy balance for a multi tubes-in-tube heat exchanger for predicting the hot side temperature profiles. Baek et al. [14] reported experiments with argon-freon

* Corresponding author.
E-mail address: matrey@iitb.ac.in (M.D. Atrey).

http://dx.doi.org/10.1016/j.cryogenics.2016.09.003
0011-2275/

Nomenclature

A	cross-sectional area (m^2)
A_G	parameter in Granryd correlation
CV	control volume
Cp	specific heat (J/kg K)
d	characteristic dimension (m)
dx	CV length (m)
f	fanning friction factor
G	mass flux (kg/m^2 s)
h	heat transfer coefficient (W/m^2 K)
H	enthalpy (J/kg)
k	thermal conductivity (W/m K)
L	length of the finned tube/external annulus (m)
l_p	wetted perimeter (m)
m	mass (kg)
$\dot{m}$	mass flow rate (kg/s)
$\dot{m}_f$	given mass flow rate (kg/s)
$\dot{m}_e$	mass flow rate at exit of inner tube (kg/s)
Nu	Nusselt number
Pr	Prandtl number
p	pressure (N/m^2)
Re	Reynolds number
SBG	Silver-Bell-Ghaly correction
T	temperature (K)
ΔT_g	temperature glide (K)
t	time (s)
V	velocity (m/s)
V_g	gas phase velocity (m/s)
V_l	liquid phase velocity (m/s)
X_{tt}	Martinelli parameter
x	Cartesian x-coordinate (m)
x_g	gas mass fraction

Greek symbols

μ	viscosity (N s/m^2)
ρ	density (kg/m^3)
τ_w	wall shear stress (N/m^2)

Subscripts

a, e	after expansion
bub	bubble point
dew	dew point
c	cold gas in the external annulus
$cond$	condensation
$crit$	critical
eq	equivalent
g	gas
h	hot gas in the inner tube
in	inlet
l	liquid
lo	liquid only
m	mixture
out	outlet
red	reduced
s	saturation
w	tube wall
$(-)$	average over CV

mixtures in a micro channel heat exchanger and concluded that the conventional two-phase heat transfer coefficient correlations can be used. Based on the experimental data reported by Nellis et al. [11] for mixtures (nitrogen-hydrocarbons), Ardhapukar et al. [15] studied the existing heat transfer correlations and modified the Granryd correlation [16] for higher mass fluxes. Ardhapurkar et al. [17] carried out a performance analysis of the recuperative heat exchanger for a MR J–T cryocooler. Ardhapurkar et al. [18] also carried out experiments on a MR J–T cryocooler with different mixtures of nitrogen-hydrocarbons and reported temperature profiles and pressure drop on both hot and cold sides of the heat exchanger. Recently, Damle et al. [19] reported a steady state analysis of a tube-in-tube heat exchanger for a MR J–T cryocooler. However, in this study the inlet temperature on the return side was fixed to the cryogenic temperature observed at steady state during experiments. The numerically predicted temperature profiles agreed reasonably well with the experimental data.

In case of non-azeotropic mixtures, the recuperative heat exchange, i.e., the boiling of low pressure stream and condensation of the high pressure stream takes place over a temperature range. This temperature range is known as the temperature glide. A large variation of thermophysical properties takes place over the temperature range of boiling/condensation. As a result, the heat transfer and the pressure drop in the heat exchanger are drastically affected. The temperature glide is a function of the mixture composition. The mixture composition also affects the lowest attainable temperature. Although there are several numerical and experimental studies on MR J–T cryocoolers, a transient study of the recuperative heat exchange has not received attention in the literature. This is due to the lack of generic correlations for boiling and condensation heat transfer with mixed refrigerants in the cryogenic temperature range.

The objective of this is to investigate the two-phase heat transfer in the recuperative heat exchanger of a MR J–T cryocooler with the available correlations in the literature. The heat transfer coefficients for boiling are estimated with the modified Granryd correlation [15]. The correlations of Shah [20], Dobson and Chato [21], and Cavallini and Zechin [22] are employed for evaluating the condensation heat transfer coefficients. A homogeneous model is used for calculating the pressure drop in the heat exchanger. A transient algorithm is developed for the resolution of heat transfer and fluid flow in the heat exchanger from ambient temperature to cryogenic temperatures. The J–T expansion of the high pressure fluid at the exit of the inner tube is also simulated for this purpose. Axial heat conduction along the inner and outer tubes, and radiative heat transfer at the surface of the outer tube is also taken into account. The numerical model is based on the finite volume method with an object-oriented modular framework. With this motive, a tube-in-tube heat exchanger is modelled in this work. For this geometrical configuration, cool down curves and temperature profiles for three different mixtures of nitrogen-hydrocarbons are available in the literature [18]. A numerical model can be very useful for predicting the heat transfer characteristics of the MR J–T cryocooler with the aim of optimizing the geometrical and operating parameters (i.e., mass flow rates, compositions and system pressure).

2. Numerical model

A computer program in C++ language has been developed for the numerical resolution of two-phase heat transfer in the recuperative heat exchanger. A one-dimensional transient model is employed for the simulation of the fluid streams and the solid tubes which together form the heat exchanger. The fluid streams and solid tubes of the heat exchanger are divided into a series of control volumes (CVs) over which the governing equations are solved. The control volume arrangement is shown in Fig. 1. A brief description of the numerical model is presented in this section.

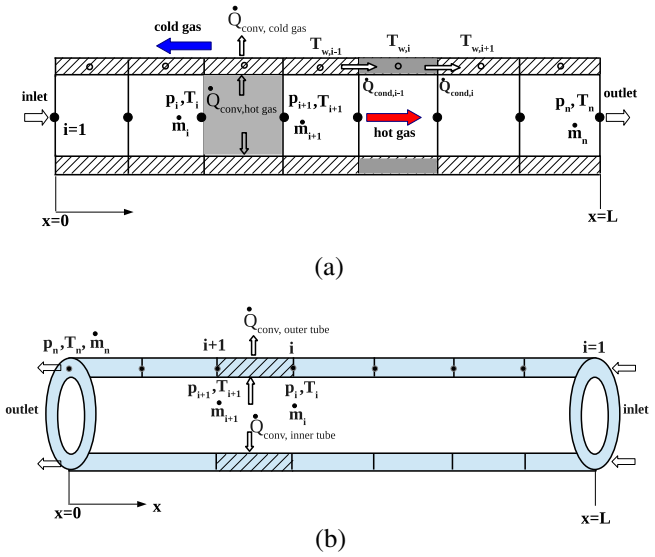

Fig. 1. CV arrangement: (a) inner fluid and inner tube; (b) outer fluid.

2.1. Assumptions

The numerical model assumes:

(i) one-dimensional heat transfer and fluid flow along the heat exchanger length;
(ii) negligible axial conduction in the fluid;
(iii) negligible body forces and axial stresses in the fluid;
(iv) adiabatic ends of inner and outer tubes;
(v) that the high and low pressures, at the inlet of the inner and outer tubes respectively, are constant during the simulation;
(vi) experimentally observed value of mass flow rate at steady state is imposed at the inlet of inner tube, thereby neglecting the mass flow rate variation during the cool down period;
(vii) constant emissivity of the outer tube receiving outside radiation at ambient temperature;
(viii) negligible effect of the helical coil on the heat transfer;
(ix) homogeneous model for pressure drop along the heat exchanger length;
(x) isenthalpic expansion of the fluid at the exit of inner tube to the pressure in the external annulus.

2.2. Governing equations

The basic equations of conservation of mass, momentum and energy for the fluid elements and energy conservation equation for solid elements are written in a differential form. The conservation of mass over a fluid CV is:

$$A\frac{\partial \bar{\rho}}{\partial t}+\frac{\partial \dot{m}}{\partial x}=0 \tag{1}$$

The conservation of momentum is given by:

$$A\frac{\partial(\bar{\rho}\bar{V})}{\partial t}+\frac{\partial(\dot{m}V)}{\partial x}=-\frac{\partial p}{\partial x}\cdot A-\tau_w l_p \tag{2}$$

The two-phase mixture velocity at a given cross-section is calculated as $V=x_gV_g+(1-x_g)V_l$ and the shear stress is calculated with the homogeneous flow model. The friction factor is evaluated based on the correlations of pipe flow considering the properties of the homogeneous two-phase mixture. The friction factor correlation employed in this work, according to the Reynolds number of the mixture [23], is given as:

$$f=\frac{16}{Re}\quad \text{for } Re<2300 \tag{3}$$

$$f=\frac{0.079}{Re^{0.25}}\quad \text{for } Re\geqslant 2300 \tag{4}$$

The energy equation for the fluid streams is resolved in terms of enthalpy and is written as:

$$A\frac{\partial(\bar{\rho}\bar{H})}{\partial t}+\frac{\partial(\dot{m}H)}{\partial x}=h\cdot l_p\cdot(T_w-\bar{T}) \tag{5}$$

A general energy equation for the solid tubes is the following:

$$\rho ACp\frac{\partial T}{\partial t}=\frac{\partial}{\partial x}\left(kA\frac{\partial T}{\partial x}\right)+\dot{Q}_{conv}+\dot{Q}_{rad} \tag{6}$$

$\dot{Q}_{conv}$ represents the heat transfer per unit length due to convection from the tube surfaces. $\dot{Q}_{rad}$ is the heat transfer per unit length due to radiation which is considered only for the outer surface of the outer tube. The variation in thermal conductivity of copper with temperature is estimated with the correlation given by Ng et al. [24]. A specific heat value of 350 J/kg K, at a mean temperature of 200 K, is taken for simulation purpose.

2.3. Boundary and initial conditions

The inner and outer solid tubes are assumed to be adiabatic at the ends. The inlet temperature, pressure and mass flow rate are known for the high pressure gas in the inner tube. From the values of temperature and pressure, the value of enthalpy at inlet $H_{h,in}$ is calculated. Thus, the boundary condition at the hot end of the heat exchanger is given as:

$$At\ x=0 \text{ and } t>0:\ \dot{m}=\dot{m}_f,\ H=H_{h,in},\ p=p_{h,in},\ \frac{dT_w}{dx}=0 \tag{7}$$

Here, $\dot{m}_f$ is the mass flow rate at the inlet of the inner tube (at $x=0$). This is a known value given in Table 3. The mass flow rate at the exit of the inner tube ($\dot{m}_e$) is different from $\dot{m}_f$ due to the transient nature of the simulation. The mass flow rate at the inlet of the external annulus is same as that at the exit of the inner tube (see Eq. (8)). The pressure at the inlet of the external annulus, i.e., the pressure after expansion is assumed to be known from the experiments and is given by $p_{c,in}$. The enthalpy at the inlet of the external annulus $H_{c,in}$ is same as that at the exit of the inner tube since expansion in the capillary tube is considered to be an isenthalpic process. $T_{a,e}$ is calculated as a function of $H_{c,in}$ and $p_{c,in}$. The value of $T_{a,e}$ reduces from ambient temperature to cryogenic temperature. Thus, boundary conditions at the cold end are imposed as:

$$At\ x=L \text{ and } t>0:\ \dot{m}=\dot{m}_e,\ H=H_{c,in},\ p=p_{c,in},\ \frac{dT_w}{dx}=0 \tag{8}$$

In addition to the boundary conditions, an initial condition is needed at time $t=0$ for a transient simulation. At time $t=0$, the pressure of the hot and cold fluid streams is initialized to $p_{h,in}$ and $p_{c,in}$ respectively. The temperature of the solid tubes is set equal the ambient temperature T_{amb} and the enthalpy of the fluid streams is set equal to the enthalpy at ambient temperature H_{amb} and corresponding pressures. Thus, we have:

$$At\ t=0 \text{ and } 0\leqslant x\leqslant L:\ \dot{m}=0,\ H=H_{amb},\ p_h=p_{h,in},\ p_c=p_{c,in} \tag{9}$$

2.4. Heat transfer correlations

There are many correlations in the literature for condensation and flow boiling heat transfer. However, their validity with

mixtures of nitrogen and hydrocarbons in the cryogenic range is not well established. Recently, Ardhapurkar et al. [15] assessed the existing flow boiling heat transfer correlations with the experimental data [11] for mixtures of nitrogen–hydrocarbons. They modified the Granryd correlation [16] and recommended its use for evaluating flow boiling of mixtures at cryogenic temperatures. The heat transfer coefficient with this correlation is estimated as:

$$h_m = h_{lo}\left(\frac{F_p}{1+A_G}\right) \tag{10}$$

where h_{lo} is the liquid only heat transfer coefficient calculated from the Dittus–Boelter equation with properties of mixture as given below.

$$h_{lo} = 0.023\left(\frac{k_l}{d}\right)\left[(1-x_g)\frac{Gd}{\mu}\right]^{0.8} Pr_l^{0.4} \tag{11}$$

where $Pr_l = \frac{\mu_l Cp_l}{k_l}$ is the liquid Prandtl number. F_p, the parameter for flow boiling of pure refrigerants, is given by:

$$F_p = 2.37\left(0.29+\frac{1}{X_{tt}}\right)^{0.85} \tag{12}$$

X_{tt}, the Martinelli parameter for turbulent–liquid and turbulent–vapour flow is calculated as:

$$X_{tt} = \left(\frac{1-x_g}{x_g}\right)^{0.9}\left(\frac{\rho_g}{\rho_l}\right)^{0.5}\left(\frac{\mu_l}{\mu_g}\right)^{0.1} \tag{13}$$

The parameter A_G in the above equation is:

$$A_G = \left(\frac{F_p}{C_{lg}}\right)x_g^2\left[\left(\frac{1-x_g}{x_g}\right)\left(\frac{\mu_g}{\mu_l}\right)\right]^{0.8}\left(\frac{Pr_l}{Pr_g}\right)^{0.4}\left(\frac{k_l}{k_g}\right)\left(\frac{Cp_g}{Cp_w}\right) \tag{14}$$

where C_{lg} is the enhancement factor to account for the gas and liquid interface effects. Granryd [16] recommended $C_{lg} = 2$ for evaporation of refrigerants. Ardhapurkar et al. [15], in the modified Granryd correlation, proposed $C_{lg} = 1.4$ for $G > 500$ kg/m^2 s. Cp_w is the apparent local specific heat for a non-azeotropic mixture and is defined as $Cp_w = \left(\frac{\partial H}{\partial T}\right)_p$.

For calculating the condensation heat transfer coefficients of the high pressure fluid, three different correlations are studied in this work. The first correlation is that of Shah [20]. This is a well known correlation for condenser calculations and is given by:

$$h_{cond} = h_{lo}\left[(1-x_g)^{0.8} + \frac{3.8\,x_g^{0.76}(1-x_g)^{0.04}}{p_{red}^{0.38}}\right] \tag{15}$$

$$h_{lo} = 0.023\left(\frac{k_l}{d}\right)Re_{lo}^{0.8} Pr_l^{0.4} \tag{16}$$

where $Re_{lo} = \frac{Gd}{\mu_l}$ and $p_{red} = \frac{p_s}{p_{crit}}$.

The second correlation is that of Dobson and Chato [21]. It is often used for mixtures and is given by:

$$Nu = 0.023 Re_l^{0.8} Pr_l^{0.4}\left[1+\frac{2.22}{X_{tt}^{0.89}}\right] \tag{17}$$

here, $Re_l = \frac{G(1-x_g)d}{\mu_l}$ and $Pr_l = \frac{\mu_l Cp_l}{k_l}$.

Finally, the correlation of Cavallini and Zecchin [22] is also employed for evaluating condensation heat transfer coefficients. This correlation, which is a modified form of the well-known Dittus-Boelter correlation, is expressed as:

$$h_{cond} = 0.05\left(\frac{k_l}{d}\right)Re_{eq}^{0.8} Pr_l^{1/3} \tag{18}$$

where Re_{eq} is the equivalent Reynolds number for two-phase flow and G_{eq} is the equivalent mass flux. These are calculated as:

$$Re_{eq} = \frac{G_{eq} d}{\mu_l} \tag{19}$$

$$G_{eq} = G\left((1-x_g) + x_g\left(\frac{\rho_l}{\rho_g}\right)^{0.5}\right) \tag{20}$$

The above condensation correlations are corrected with the Silver [25] and Bell and Ghaly [26] (SBG) method to account for the non-isothermal condensation process of mixtures. Several researchers [27–29] have applied the SBG correction to refrigerant mixtures. The corrected heat transfer coefficient (h_m) is evaluated as:

$$\frac{1}{h_m} = \frac{1}{h_{cond}} + \frac{Z_g}{h_g} \tag{21}$$

Here, h_g is the vapour only heat transfer coefficient calculated with the Dittus-Boelter equation as:

$$h_g = 0.023\left(\frac{k_g}{d}\right)Re_g^{0.8} Pr_g^{0.4} \tag{22}$$

where $Re_g = \frac{x_g Gd}{\mu_g}$ and $Pr_g = \frac{\mu_g Cp_g}{k_g}$. The parameter Z_g is the ratio of the sensible cooling of the vapour to the total cooling rate and is given by:

$$Z_g = x_g Cp_g \frac{dT_{dew}}{dH} \approx x_g Cp_g \frac{\Delta T_g}{\Delta H_m} \tag{23}$$

where Cp_g is the specific heat of gas phase and $\frac{dT_{dew}}{dH}$ is the slope of the dew point temperature curve with respect to mixture enthalpy. This is approximated by the ratio of temperature glide ΔT_g and enthalpy of isobaric condensation of the mixture, ΔH_m.

2.5. Numerical resolution

For the numerical resolution of the governing equations, the fluid streams are divided into a series of control volumes (CVs) along their length as shown earlier in Fig. 1. For both the hot and cold fluid streams, the variables (e.g. p, H, $\dot{m}$) are known at the inlet cross-section as indicated previously by the boundary conditions. Therefore, a step-by step method is suitable here for the resolution of the fluid streams. In the step-by-step method, from the values of the variables at a given cross-section, the values at the next cross-section are evaluated iteratively. Thus, marching in the flow direction is possible to obtain the variable values along the heat exchanger length. For the solid tubes, integration of Eq. (6) over a CV results in a system of linear algebraic equations. TDMA (Tri-Diagonal Matrix Algorithm) method is used for solving the system of equations. Within the global transient algorithm, each time step is converged before going to the next time step. At every time step, the fluid streams and solid elements are resolved simultaneously in an iterative way until convergence is attained at that time step. Iterations at every time step are carried out until the maximum absolute differences of all the variables along the heat exchanger length, in consecutive iterations, are less than 1.0×10^{-3}. After, the time step has converged, the initial map is updated and the next time step calculation begins. When the maximum absolute differences of all the variables along the heat exchanger length, between two consecutive time steps, are less than 1.0×10^{-3}, steady state is declared. The simulations are carried out with grid sizes of 150 CVs, 300 CVs and 450 CVs. It was observed that there are no significant differences in the temperature profiles obtained with grid sizes of 300 Cvs and 450 CVs. The results reported in this work are with a grid size of 300 CVs along the heat exchanger length.

3. Experimental set-up and heat exchanger configuration

The experimental set-up with the heat exchanger amongst other devices and instrumentation is shown in Fig. 2. The uncertainties of the temperature sensors are obtained by combining systematic and random uncertainties assuming Student's *t*-distribution with 95% confidence limit. The expanded uncertainties in the temperatures vary in the range of ±0.59 °C to ±0.65 °C. The uncertainty in the measurement of mass flow rate and pressures are around ±1.66%. Temperature sensors were installed on both the inner and outer tubes for measuring the temperatures along the length of the heat exchanger. Fig. 3 shows the pictorial view of the helically coiled tube-in-tube heat exchanger. The length of the heat exchanger is 15 m. In Fig. 3, the overall height of the heat exchanger assembly is around 650 mm. The sensors are installed on both inner and outer tubes of this heat exchanger, however,they are not visible in the photograph. More details of the devices and instrumentation for experiments can be found in the work reported by Ardhapurkar et al. [18]. Table 1 specifies the geometrical parameters of the heat exchanger. The gas mixture at ambient temperature enters the inner tube of the heat exchanger at pressures of around 10–20 bar. After expansion, the low pressure gas mixture at around 4–6 bar flows through the external annulus in the opposite direction. This results in a counter-flow heat exchanger. The inlet temperature of the low pressure fluid depends on the mixture composition and varies in the range of 90–150 K. The high pressure fluid stream (hot side) condenses inside the inner tube while the low pressure fluid stream (cold side) evaporates in the external annulus.

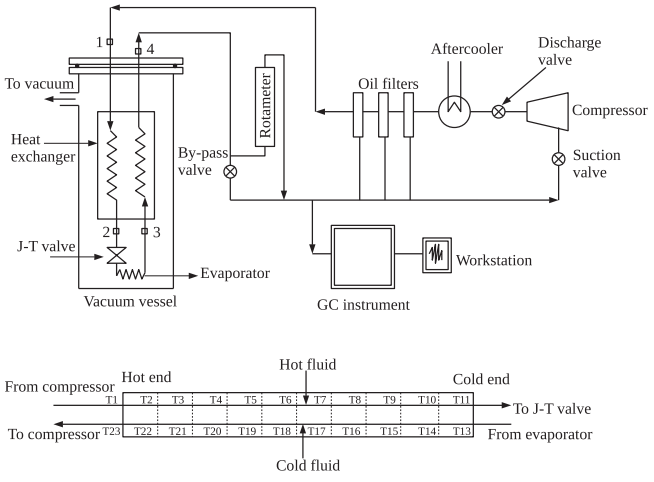

Fig. 2. Experimental set-up [18].

Fig. 3. Photograph of the heat exchanger [18].

4. Results and discussion

Numerical simulations, with the aforementioned transient numerical model, are carried out with three different mixtures (Mix#1, Mix#2 and Mix#3). The numerical results are compared with the experimental data [18] for these mixtures. The mixture compositions in circulation are specified in Table 2. The thermophysical properties of the mixture are evaluated, at the local conditions of temperature and pressure along the heat exchanger, using the Peng-Robinson equation of state in the aspenONE software [30]. The lowest attainable temperature is affected by the relative percentage of the mixture constituents. Mix#2 with the highest percentage of nitrogen yielded the lowest temperature below 100 K. Table 3 gives the operating parameters for all the three cases simulated in this work. This table gives the experimental values of mass flow rates, pressures and temperature at the inlet and outlet of the hot and cold sides of the heat exchanger. In Fig. 2, the end pressures on the hot side i.e., $p_{h,in}$ and $p_{h,out}$ are measured at locations 1 and 2 respectively. Similarly, the end pressures on the cold side, $p_{c,in}$ and $p_{c,out}$, are measured at locations 3 and 4 respectively. For all the cases, the heat transfer coefficients for flow boiling are estimated using modified Granryd correlation [15] which was obtained by analyzing experimental data provided by Nellis et al. [11] for six different mixtures of nitrogen-hydrocarbons. The correlations of Shah [20], Dobson and Chato [21], and Cavallini and Zechin [22] are employed for evaluating the condensation heat transfer coefficients. This is because the average values of the overall heat transfer coefficients predicted with these correlations were in fair agreement with the experimentally calculated values [17].

It should be noted that the values of inlet pressures and mass flow rates on the hot and cold sides will vary during the transient

Table 1
Dimensions of the helically coiled heat exchanger [18].

Parameter	Size (mm)
Inner tube, ID (mm)	4.83
Inner tube, OD (mm)	6.35
Outer tube, ID (mm)	7.89
Outer tube, OD (mm)	9.52
Length of heat exchanger (m)	15
Coil diameter (mm)	200
Coil pitch (mm)	14.5
Number of turns	23

Table 2
Mixture compositions and lowest temperature ranges [18].

Mixture	Composition (% mol) ($N_2/CH_4/C_2H_6/C_3H_8/iC_4H_{10}$)	Temperature range (K)
Mix#1	6.99/46.335/33.533/3.996/9.146	140–150
Mix#2	39.86/16.865/12.845/17.38/13.045	<100
Mix#3	18.455/32.785/16.05/20.14/12.57	110–120

Table 3
Operating parameters for different mixtures [18].

Mixture	T_{low} (K)	$\dot{m}$ (g/s)	$p_{h,in}$ (bar)	$T_{h,in}$ (K)	$p_{c,in}$ (bar)	$T_{c,in}$ (K)	$p_{h,out}$ (bar)	$p_{c,out}$ (bar)
Mix#1	143.98	3.80	12.38	303.18	6.11	144.87	11.41	3.2
Mix#2	98.62	3.70	14.74	301.50	5.61	100.17	13.95	2.6
Mix#3	113.45	2.64	11.70	302.66	5.57	114.83	11.01	2.3

period. Simulation of the compressor and the capillary device is required to take care of the changing pressure ratios and the corresponding mass flow rates. However, the main focus of this work is to study the transient behaviour of the heat exchanger for different mixture compositions using the correlations mentioned above. The validity of these correlations in the cryogenic range for mixtures of nitrogen-hydrocarbons is not well established. In this study, the values of pressures at the inlet of the inner and outer annulus, and the mass flow rate at the inlet of the inner tube are assumed to be constant. These values are set equal to the representative values at steady state as shown in Table 3.

It may be noted that the numerical model developed in this work has a transient nature. Therefore, the steady state is obtained by marching in time from the initial conditions at time $t = 0$. The transient evolution of temperatures and gas mass fraction (x_g) on the hot and cold sides for Mix#1 are shown in Figs. 4 and 5 respectively. At time $t = 0$, the temperature map for both the fluids in the tubes and the solid tubes is initialized to ambient temperature condition. The corresponding gas mass fraction of both fluid streams is unity, i.e., single phase gas condition. At time $t > 0$, mass flow rate is imposed at the inlet cross sections of the inner tube. The mass flow rate at the inlet of the external annulus is the same as that at the exit of the inner tube after isenthalpic expansion. The high pressure fluid at the outlet of the inner tube starts cooling due to the J–T effect. As a result, the inlet temperature on the cold side starts reducing. Thereafter, due to subsequent expansions and heat transfer in the heat exchanger, the temperatures of both the high and low pressure fluid streams continue to decrease. The gas mass fractions towards the cold end of the heat exchanger also start reducing due to condensation and boiling of hot and cold streams respectively. This process continues until a steady state is reached, i.e., when the temperature profiles of the hot and the cold fluid do not change with time. With a time step of one second, temperature profiles are constantly generated and saved. It can be seen from Fig. 4 that after 70 min the cold end temperature has reached its lowest value. However, as the temperature profiles are changing from 70th minute to 80th minute the simulation continues for the selected convergence criteria discussed earlier. The steady state is achieved after 83.49 min. The temperature profiles at steady state match exactly with those after 80 min. This indicates that the criteria for declaring steady state is satisfactory. The same is observed with the profiles of gas mass fraction shown in Fig. 5. The simulations are also carried out with different number of CVs along the heat exchanger length to ensure mesh independent results. Table 4 shows the temperature and pressure values at the outlet of hot and cold sides for three different mesh sizes. It is seen that there is no significant variation of the output parameters with CV number. For this study, simulations with different time steps were worked out. With small time steps, of the order of 0.1 s, 0.5 s, 1 s, no significant differences were observed in the transient evolution. However, with higher time steps of 10 s or 100 s, each time step convergence could not be achieved. The drastic change of physical properties due to phase change could be a reason for the same. Therefore, to converge each time step a time step of 1 s was employed in this work.

Fig. 6 shows the comparison of the numerical and experimental temperature profiles of the hot and cold fluid for Mix#1. On the hot side, the gas mixture enters as single phase gas at an ambient temperature of 303.18 K and leaves the heat exchanger as two-phase fluid at around 152 K. The cold fluid enters the heat exchanger in a two-phase state at 144 K and leaves as single phase gas at around 296 K. Although the outlet temperature on the hot and cold sides match well, the predicted temperature profiles show a large deviation from the experimental observation in the middle portion of the heat exchanger. The numerical predictions are on the higher side and the extent of the single phase region from the hot end of the heat exchanger is larger as compared to the experimental data. The single phase region, seen by the change of slope in both Fig. 6a and b, starts at a length of around 10.5 m measured from the low temperature side in the experimental observation. In case of numerical prediction, this region starts from around 7.5 m. It is observed that the temperature profiles, with Shah [20], Dobson and Chato [21], and Cavallini and Zecchin [22] correlation, differ slightly in the central portion near the transition region. The temperature profiles overlap in the single phase gas region and towards the cold end of the heat exchanger. The maximum relative difference between the numerical and experimental values of temperature along the hot side is around 14.89%, while the same on

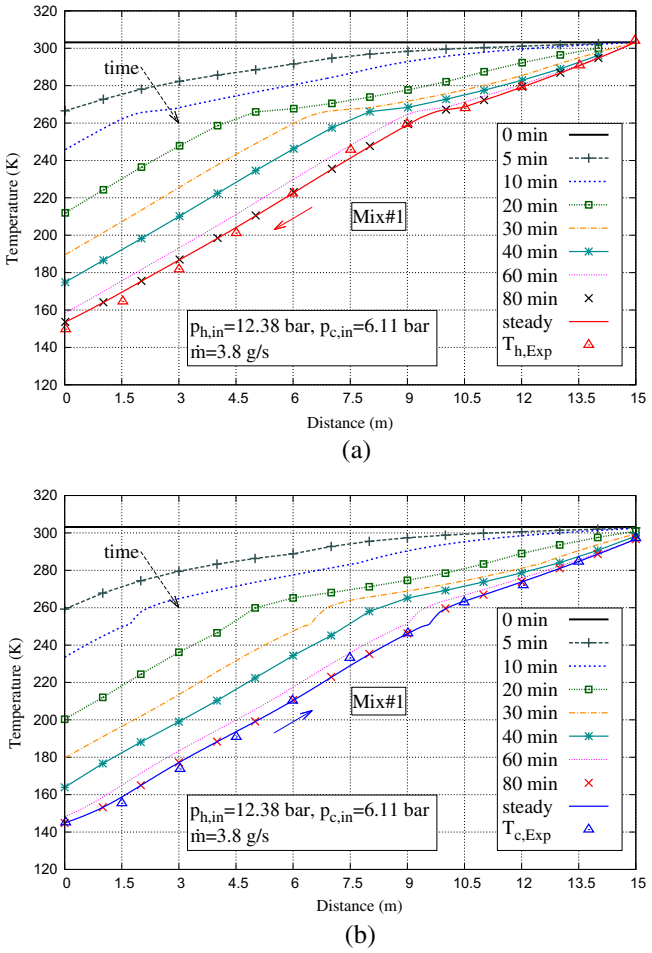

Fig. 4. Transient evolution of temperature profiles for Mix#1: (a) hot side; (b) cold side.

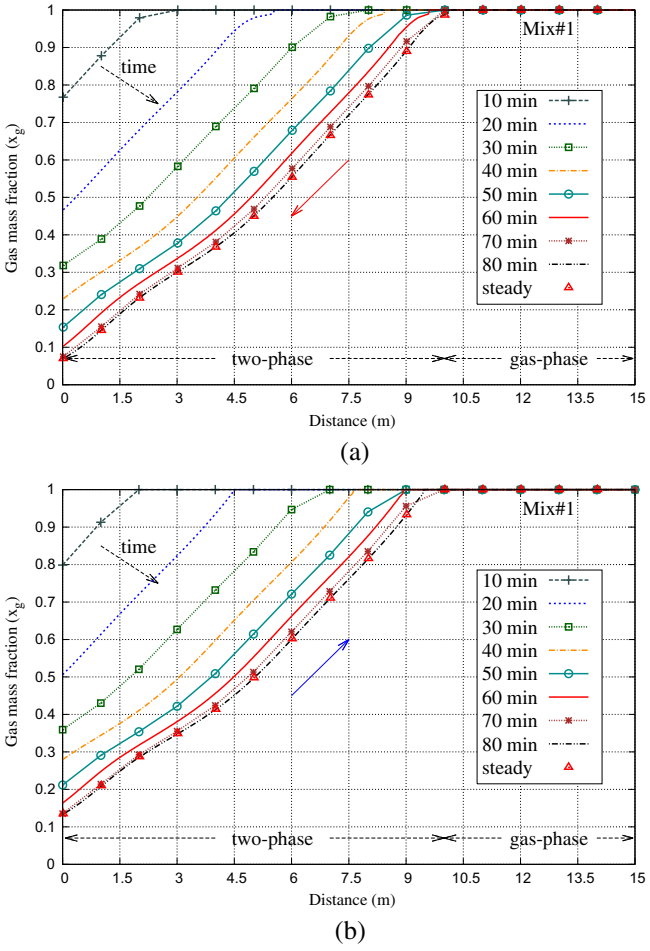

Fig. 5. Transient evolution of gas mass fractions for Mix#1: (a) hot side; (b) cold side.

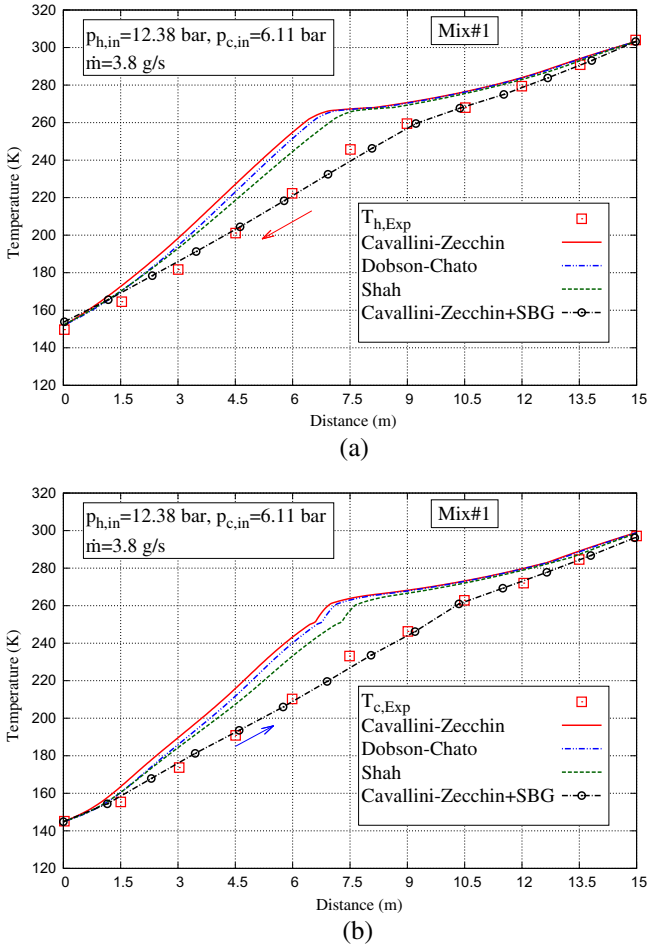

Fig. 6. Temperature profiles for Mix#1: (a) hot side; (b) cold side.

Table 4
Outlet temperatures and pressures with mesh size for Mix#1.

CVs	$T_{h,out}$ (K)	$p_{h,out}$ (bar)	$T_{c,out}$ (K)	$p_{c,out}$ (bar)
150	153.375	12.111	296.606	2.2456
300	153.391	12.109	296.607	2.2439
450	153.385	12.108	296.602	2.2451

the cold side is around 16.09%. However, when SBG correction is applied to the condensation correlations, the numerical temperature profiles match very well with the experimental data. In this case, the maximum relative differences of temperature on the hot and cold sides are 2.42% and 2.58% respectively. Therefore, the SBG correction works well for Mix#1. Although Fig. 6a and b shows the temperature profiles with SBG correction applied to Cavallini and Zecchin [22] correlation, similar results are obtained with the other two correlations with the SBG correction. The same are not included here for clarity of the figure.

Fig. 7 shows the heat transfer coefficients on the hot side calculated with Shah [20], Dobson and Chato [21], Cavallini and Zecchin [22], and Cavallini and Zecchin [22] with SBG correction. The flow boiling heat transfer coefficient on the cold side, estimated with the modified Granryd correlation [15], is also shown in Fig. 7. It is observed that when SBG correction is applied to the Cavallini and Zecchin [22] correlation, the heat transfer coefficients reduce drastically. In this case, due to the lower heat transfer coefficients the location of transition region is shifted to towards the hot end of

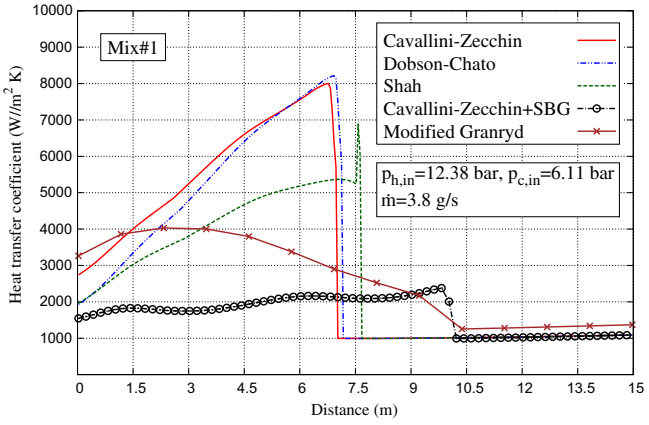

Fig. 7. Heat transfer coefficients on the hot and cold sides for Mix#1.

the heat exchanger. As a result, the location of the transition region to/from single phase (in Fig. 6) is also captured well with the SBG correction along with the agreement of predicted temperatures with the experimental data.

Fig. 8 shows the comparison between numerically and experimentally obtained temperature profiles for Mix#2. At the hot end of the heat exchanger, the gas mixture is in single phase state while it is in a two-phase condition at the cold end in both the inner and outer tubes. In this case, it is observed that with the SBG correction applied to Cavallini and Zecchin [22] correlation, the lowest pre-

dicted temperature of the cold end does not drop below 130 K. However, the temperature variations towards the hot end of the heat exchanger, close to the phase change region, compare well with the SBG correction. This is true for both the hot and cold streams. During experimentation with Mix#2, the lowest temperature attained at the cold end is around 100 K. In the numerical simulations, the cold end temperature dropped to 100 K only when the SBG correction was not applied to the condensation correlations. Near the transition region the maximum relative differences of temperature on the hot and cold sides are 6.50% and 11.16% respectively. Towards the cold end of the heat exchanger, the relative differences of temperature on the hot and cold side are about 5.3% and 4.9% respectively. Thus, apart from the transition region, the predictions without the SBG correction match reasonably well with the experimental data on the colder side of the heat exchanger. Fig. 9 shows the heat transfer coefficients on the hot and cold sides. It can be observed that the two-phase heat transfer coefficients, usually higher than those in the single phase, are comparable. For Mix#2, the use of SBG correction results in lower heat transfer coefficients as compared to Mix#1. Due to this reason, the lowest temperature (around 100 K) cannot be achieved with SBG correction. The temperature profiles and the heat transfer coefficients for Mix#3 are shown in Figs. 10 and 11 respectively. From a single phase state at 302 K the gas mixture on the hot side condenses in the inner tube and exits at around 119 K. The return side fluid enters in two-phase condition at 114 K and leaves as single phase gas at 298 K. For Mix#3 also, the lowest temperature observed in the experiments (around 114 K) cannot be obtained using SBG correction for condensation correlations. Nevertheless,

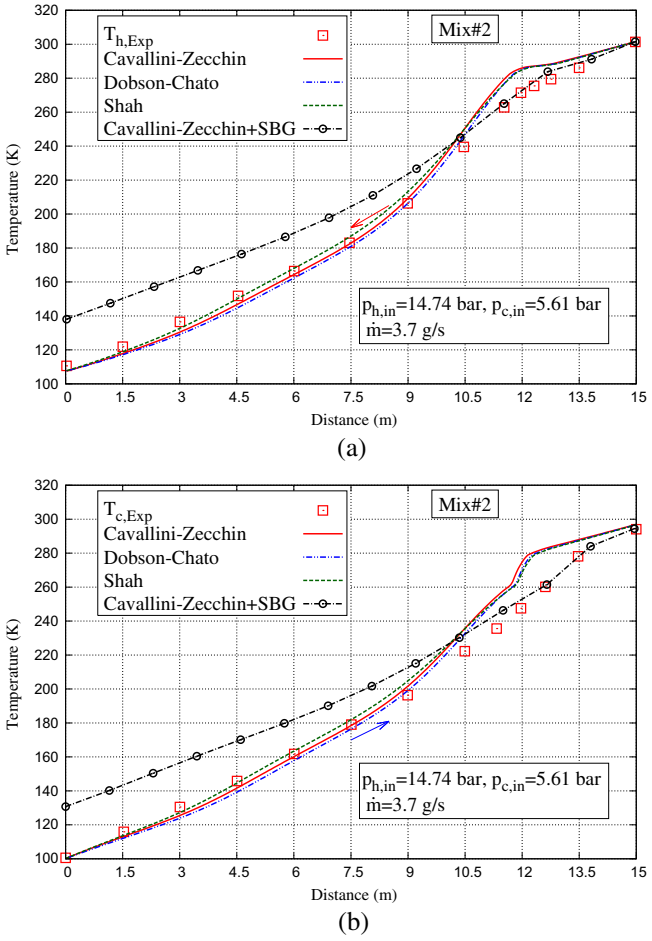

Fig. 8. Temperature profiles for Mix#2: (a) hot side; (b) cold side.

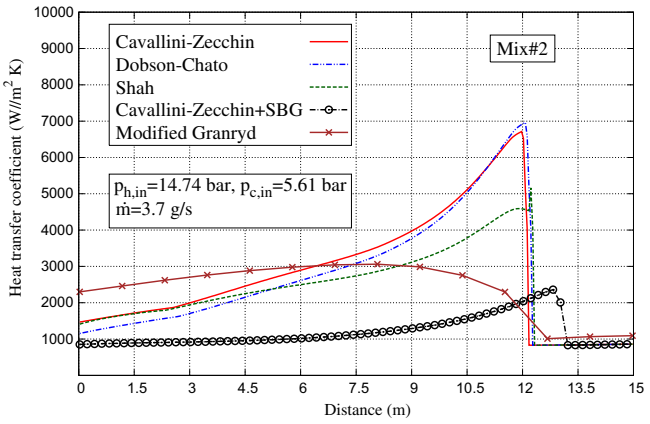

Fig. 9. Heat transfer coefficients on the hot and cold sides for Mix#2.

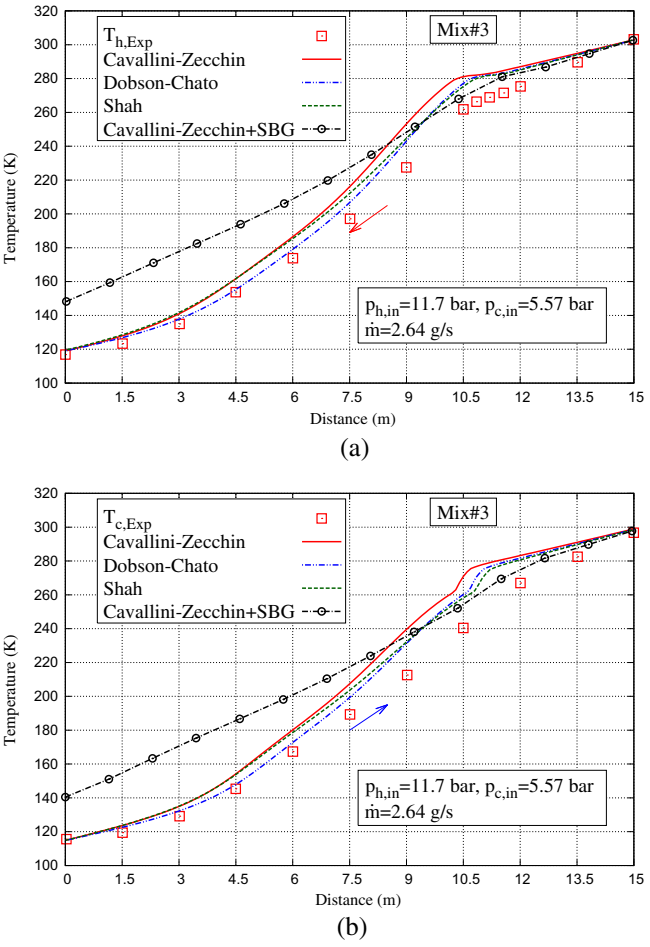

Fig. 10. Temperature profiles for Mix#3: (a) hot side; (b) cold side.

as in case of Mix#2, it is seen that the prediction with SBG correction is better near the single phase region. The experimentally observed lowest temperature is obtained using condensation correlations without the SBG correction. In this case, near the single phase gas region, the maximum relative differences of temperature along the hot and cold sides are around 11.36% and 12.63% respectively. However, towards the cold end of the heat exchanger the relative differences of temperature on the hot and cold sides are about 5.4% and 5.97% respectively. For Mix#3 also, the temperature profiles agree well with the experimental data except in the region

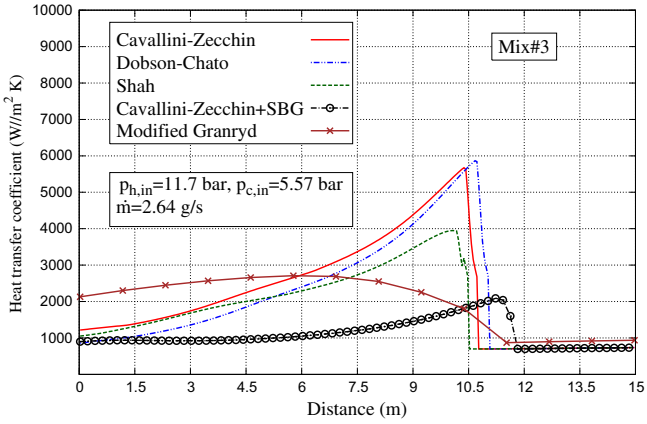

Fig. 11. Heat transfer coefficients on the hot and cold sides for Mix#3.

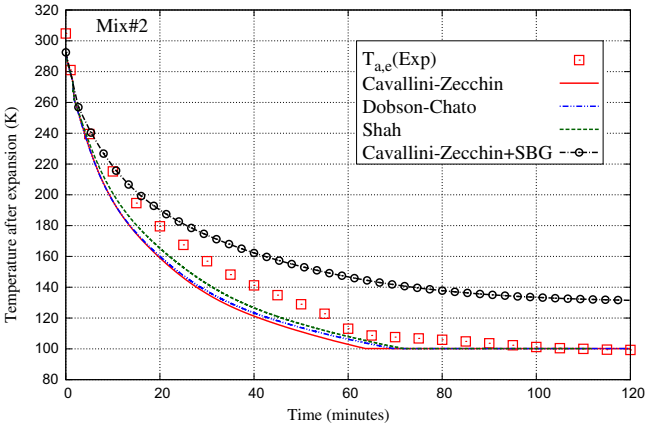

Fig. 13. Cool down curve for Mix#2.

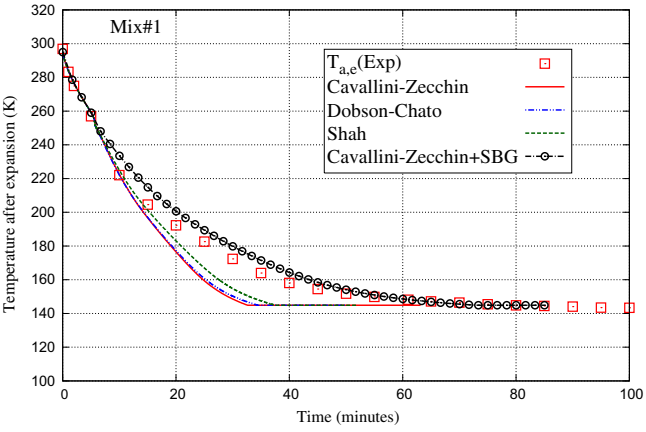

Fig. 12. Cool down curve for Mix#1.

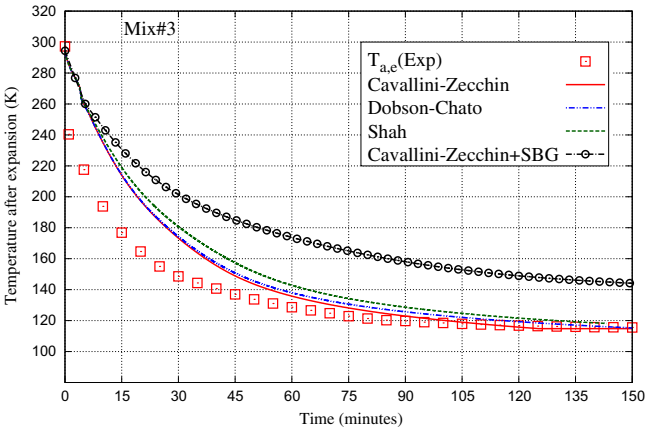

Fig. 14. Cool down curve for Mix#3.

of transition to single phase. For both Mix#2 and Mix#3, the change in slope of the temperature profiles near the cold end is very well predicted by the numerical model. For the cases studied in this work, with lowest temperatures in the range of 100–140 K, the effect of radiation is found to be insignificant. The relative difference in the hot side outlet temperature with and without radiative heat transfer at the outer surface of the outer tube is 0.22%. The same in case of the temperature after expansion is about 0.16%. This can be attributed due to the low emissivity of copper (ϵ = 0.059) and the multi-layer insulation which reduces the temperature differential.

The cool down curves for Mix#1, Mix#2 and Mix#3 are shown in Figs. 12–14 respectively. For Mix#1, with the SBG correction the predicted cool down curve agrees well with the experimental data. For Mix#2 and Mix#3, with SBG correction, the temperature after expansion does not drop below 140 K. Using condensation correlations without the SBG correction, the experimentally observed lowest temperature is obtained in both the cases. Unlike Mix#1, the cool down curves do not match well for Mix#2 and Mix#3. After a time period of around 60 min, the numerically predicted curve comes closer to the experimental values and match well thereafter. The overall cool down time for reaching the steady state is predicted well by the numerical model. It is clear from the simulations that the prediction of heat transfer coefficients is crucial to the transient evolution of the heat exchanger. The heat transfer coefficients are affected by the mixture composition and the operating conditions like pressure and mass flow rate. For example, in case of Mix#3, the mass flux of the hot stream is 144 kg/m^2 s while that of Mix#1 and Mix#2 are 208 kg/m^2 s and 202 kg/m^2 s, respectively. Therefore, in case of Mix#3, the heat transfer coefficients are relatively lower as compared to Mix#1 and Mix#2. It is evident that the usually employed SBG correction for prediction of condensation heat transfer coefficients cannot be applied to all mixtures. The SBG correction reduces the heat transfer coefficients drastically and this reduction depends on the temperature glide and thermophysical properties of the mixture. It can be seen from Eqs. (19) and (21) that higher temperature glide results in lower heat transfer coefficients when SBG correction is employed. The temperature glides for all the mixtures are shown in Table 5. The temperature glide is lowest for Mix#1 (130.84 K) as compared to Mix#2 (183.54 K) and Mix#3 (170.82 K). The temperature glides for mixtures Mix#2 and Mix#3 are close to each other. The application of SBG correction to Mix#2 and Mix#3 results in heat transfer coefficients which are comparable to those in the single phase region (see Figs. 9 and 11). As a result, the cold end temperature does not drop to the values observed in the experiments. However, the reduction in the heat transfer coefficients with the SBG correction, improves the predictions near the change of phase region for all the mixtures. For Mix#2 and Mix#3 it is seen that the numerical predictions without the SBG correction, agree well towards the cold end of the heat exchanger but deviate near the transition to the single phase region. One of the reasons for this is the large variation of thermophysical properties due to higher temperature glide. Also, the flow boiling heat transfer correlation is affected by the temperature glide and is more accurate when the mass fraction x_g is in the range of 0.1–0.75 [15].

Table 5
Temperature glide of different mixtures.

Mixture	Hot side temperatures (K)			Cold side temperatures (K)		
	T_{bub}	T_{dew}	ΔT_g	T_{bub}	T_{dew}	ΔT_g
Mix#1	139.29	267.64	128.35	114.62	245.46	130.84
Mix#2	103.61	287.15	183.54	86.74	253.77	167.03
Mix#3	110.97	281.79	170.82	92.42	253.56	161.14

Table 6
Comparison of outlet temperatures of hot and cold fluid streams.

Observation	$T_{h,out}$(K)			$T_{c,out}$(K)		
	Mix#1	Mix#2	Mix#3	Mix#1	Mix#2	Mix#3
Experimental	149.29	110.53	116.26	296.89	293.50	296.16
Cavallini-Zecchin [22]+(SBG)	153.391	137.652	147.802	296.607	294.907	298.011
Cavallini-Zecchin [22]	151.552	107.245	118.681	299.00	296.919	298.963
Dobson-Chato [21]	151.774	107.408	118.966	298.896	296.782	298.734
Shah [20]	152.006	107.487	119.207	298.502	296.705	298.589

The differences in the prediction of the cool down curve are due to the fact that the 2 m long capillary tube has not been simulated in the present work. As the focus is on the simulation of the heat exchanger, isenthalpic expansion of the fluid from its state before the expansion to the pressure in the external annulus is considered in this work. A more detailed model is needed to simulate the entire cryocooler by taking into account the effect of the compressor and the capillary tube in the transient system. This will take care of the changing pressures and mass flow rate during the transient period.

Considering the lack of generic correlations for mixtures in the cryogenic range, the current work is an attempt to capture the transient evolution of the recuperative heat exchanger in MR J–T cryocoolers with the existing correlations. However, on a global basis, it is observed from the numerical simulations that the overall heat transfer in the heat exchanger is predicted well by all the correlations employed in this work. This is reflected by the outlet temperature values for hot and cold streams in Table 6. The outlet temperatures of the hot and cold streams agree well with the experimental data. The relative differences in the numerical and measured values of outlet temperatures are below 3%. Also, the overall cool down time is predicted reasonably well by the numerical model. Further work is necessary to develop more accurate heat transfer correlations for which more experimental data is necessary.

5. Conclusions

Transient simulation of the recuperative heat exchange in a mixed refrigerant J–T cryocooler is presented in this paper. A one-dimensional transient model has been developed for the simulation of the two-phase heat transfer. Physical property variation of the mixtures with temperature and pressure is taken into account. Axial conduction in the solid tubes and radiative heat transfer from the outer tube is also considered. For the transient evolution of the heat exchanger, from ambient conditions to the cryogenic temperatures, the J–T expansion is simulated. The heat transfer coefficients for flow boiling are calculated with the modified Granryd correlation [15] while correlations of Cavallini and Zecchin [22], Dobson and Chato [21] and Shah [20] are used to evaluate the condensation heat transfer. Simulations with and without the SBG correction, applied to the condensation heat transfer coefficients, are also carried out.

The numerical results for three different nitrogen-hydrocarbons mixtures are compared with the experimental data. It is observed that the SBG correction reduces the heat transfer coefficients drastically. For Mix#1 with low temperature glide, the use of SBG correction gives good results. With the SBG correction in case of Mix#2 and Mix#3, the cold end temperature does not drop to the value observed in the experiments. Therefore, it can be concluded that the SBG correction method gives good predictions of heat transfer coefficients for mixtures with relatively low temperature glide.

The overall heat transfer in the heat exchanger is predicted reasonably well with correlations studied in this work. The relative differences between the experimental and numerical values of outlet temperatures are less than 3% for all the three mixtures. The overall cool down time and the qualitative trends in the temperature profiles of both hot and cold fluid streams are also predicted reasonably well by the numerical model.

References

[1] Brodyanskii VM, Gromov EA, Grezin AK, Yagodin VM, Nikolaskii VA, Tashchina DG. Efficient throttling cryogenic refrigerators which operate on mixtures. Chem Pet Eng 1971;7(12):1057–61.
[2] Longsworth RC, Boiarski MJ, Klusmier LA. 80 K closed cycle throttle refrigerator. Cryocoolers 1995;8:537–41.
[3] Walimbe NS, Narayankhedkar KG, Atrey MD. Experimental investigation on mixed refrigerant Joule–Thomson cryocooler with flammable and nonflammable refrigerant mixtures. Cryogenics 2010;50(10):653–9.
[4] Alexeev A, Haberstroh Ch, Quack H. Further development of a mixed gas Joule–Thomson refrigerator. Adv Cryog Eng 1998;43:1667–74.
[5] Keppler F, Nellis G, Klein SA. Optimization of the composition of a Gas mixture in a Joule–Thomson cycle. HVACR Res 2004;10(2):213–30.
[6] Gong MQ, Luo EC, Zhou Y, Liang JT, Zhang L. Optimum composition calculation for multicomponent cryogenic mixture used in Joule–Thomson refrigerators. Adv Cryog Eng 2000;45:283–90.
[7] Lakshmi Narasimhan N, Venkatarathnam G. Effect of mixture composition and hardware on the performance of a single stage J–T refrigerator. Cryogenics 2011;251(8):446–51.
[8] Maytal B-Z. Hampson's type cryocoolers with distributed Joule–Thomson effect for mixed refrigerants closed cycle. Cryogenics 2014;61:92–6.
[9] Tzabar N. Binary mixed-refrigerants for steady cooling temperatures between 80 K and 150 K with Joule–Thomson cryocoolers. Cryogenics 2014;64:70–6.
[10] Gong MQ, Wu JF, Luo EC, Qi YF, Hu QG, Zhou Y. Study on the overall heat transfer coefficient for the tube-in-tube heat exchanger used in mixed-gases coolers. Adv Cryog Eng 2002;47B:1483–90.
[11] Nellis G, Hughes C, Pfotenhauer J. Heat transfer coefficient measurements for mixed gas working fluids at cryogenic temperatures. Cryogenics 2005;45(8):546–56.
[12] Alexeev A, Thiel A, Haberstroh Ch, Quack Q. Study of behavior in the heat exchanger of a mixed gas Joule–Thomson cooler. Adv Cryogenic Eng 2000;45:307–14.
[13] Ardhapurkar PM, Sridharan A, Atrey M. Investigations on two-phase heat exchanger for mixed refrigerant Joule–Thomson cryocooler. Adv Cryogenic Eng 2012;57A:706–13.
[14] Baek S, Lee C, Jeong S. Investigation of two-phase heat transfer coefficients of argon-freon cryogenic mixed refrigerants. Cryogenics 2014;64:29–39.
[15] Ardhapurkar PM, Sridharan A, Atrey M. Flow boiling heat transfer coefficients at cryogenic temperatures for multi-component refrigerant mixtures of nitrogen-hydrocarbons. Cryogenics 2014;59:84–92.

[16] Granryd E. Heat transfer in flow evaporation of non-azeotropic refrigerant mixtures – a theoretical approach. Proc 18th int congress of refrigeration, Montreal, vol. 3. p. 1330–4.
[17] Ardhapurkar PM, Sridharan A, Atrey M. Performance evaluation of heat exchanger for mixed refrigerant J–T cryocooler. Cryogenics 2014;63:49–56.
[18] Ardhapurkar PM, Sridharan A, Atrey M. Experimental investigation on temperature profile and pressure drop in two-phase heat exchanger for mixed refrigerant Joule–Thomson cryocooler. Appl Therm Eng 2014;66:94–103.
[19] Damle RM, Ardhapurkar PM, Atrey MD. Numerical analysis of the two-phase heat transfer in the heat exchanger of a mixed refrigerant Joule-Thomson cryocooler. Cryogenics 2015;72:103–10.
[20] Shah MM. A general correlation for heat transfer during film condensation inside pipes. Int J Heat Mass Transf 1979;22:547–56.
[21] Dobson MK, Chato JC. Condensation in smooth horizontal tubes. J Heat Transf Trans ASME 1998;120:193–213.
[22] Cavallini A, Zecchin R. A dimensionless correlation for heat transfer in forced convection condensation. Proceedings of the 6th int heat transfer conference, Tokoyo, vol. 3. p. 309–13.
[23] Douglas JF, Gasiorek JM, Swaffield JA. Fluid mechanics. 3rd ed. Harlow: Addison-Wesley; 1999.
[24] Ng KC, Xue H, Wang JB. Experimental and numerical study on a miniature Joule-Thomson cooler for steady-state characteristics. Int J Heat Mass Transf 2002;45:609–18.
[25] Silver L. Gas cooling with aqueous condensation. Trans Inst Chem Eng 1947;25:30–42.
[26] Bell KJ, Ghaly MA. An approximate generalized design method for multicomponent/partial condenser. AIChE Symp Ser 1973;69:72–9.
[27] Cavallini A, Col DD, Doretti L, Matkovic M, Rossetto L, Zilio C. Condensation in horizontal smooth tubes: a new heat transfer model for heat exchanger design. Heat Transf Eng 2006;27(8):31–8.
[28] Col DD, Cavallini A, Thome JR. Condensation of zeotropic mixtures in horizontal tubes: new simplified heat transfer model based on flow regimes. J Heat Transf 2005;127:221–30.
[29] Shah MM. An improved and extended general correlation for heat transfer during condensation in plain tubes. HVAC&R Res 2009;15(5):889–913.
[30] aspenONE V 7.1. Aspen Technology Inc, Burlington, MA 01803, USA; 2009.